International Journal of Industrial Chemistry (IJIC)
a SpringerOpen Journal

RESEARCH Open Access

Kinetics of the Fischer-Tropsch synthesis on silica-supported cobalt-cerium catalyst

Mohsen Mansouri[1], Hossein Atashi[1*], Ali Akbar Mirzaei[2] and Reza Jangi[1]

Abstract

Background: The process of converting synthesis gas into liquid fuels (Fischer-Tropsch synthesis) is a well-known technology. Among all Fischer-Tropsch synthesis (FTS) catalysts, Co- and Fe-based ones are applicable for industrial processes due to their low cost and high activity and selectivity. In this experimental study, a kinetic model has been developed for FTS reactions using co-precipitation technique and Co-Ce/SiO_2 as the catalyst.

Results: Rate data have been obtained for CO hydrogenation over a co-precipitated well-characterized Co-Ce/SiO_2 catalyst, studied in a fixed-bed micro-reactor at atmospheric pressure under the conditions of 200°C to 300°C, H_2/CO feed ratio (mol/mol) of 1 and 1.5, and space velocity in the range 2,700 to 5,200 h^{-1}. Characterization of both precursor and calcined catalysts was carried out using powder X-ray diffraction, scanning electron microscopy, and Brunauer-Emmett-Teller surface area measurements.

Conclusions: The kinetic parameters were estimated with nonlinear regression method. The data were best fitted by a Langmuir-Hinshelwood-Hougen-Watson approach. The activation energy for the optimal kinetic model was determined to be 31.57 kJ mol^{-1}.

Keywords: Fischer-Tropsch synthesis, Kinetic modeling, LHHW

Background

Fischer-Tropsch synthesis (FTS), the production of liquid hydrocarbons from synthesis gas (CO and H_2) at atmospheric pressure or above and at a few hundred degrees Celsius, is a promising developing option for the environmentally sound production of chemicals and fuels from coal and natural gas [1,2]. Considerable progress has been made in the past two decades in the development of more active and selective cobalt and iron catalysts and more effective reactor/process technologies [3]. The FTS with cobalt catalysts is not complicated by extensive, irreversible changes in the catalyst. With iron catalysts, however, their physical and chemical nature is considerably altered by wax and carbon deposition and by formation of carbides and magnetite [4]. Cobalt-based catalysts are the preferred catalysts for hydrocarbon synthesis because of their high FTS activity, selectivity for long-chain paraffins, and low activity for the water-gas shift reaction [5]. Supported Co catalysts with high specific rates require the synthesis of small metal crystallites at high local surface densities on support and the use of supports or alloys that increase the rate per surface Co (turnover rate). It has been reported that the cobalt and cerium matrix plays a synergistic role in the chemisorption of reactant molecules, thereby controlling the reactivity of the title system in the FTS reaction [6]. Co-Ce catalysts have been investigated for their selectivity for lower molecular weight olefins [7-9]. Mixed cobalt-cerium oxide catalysts supported by SiO_2 [10,11] and TiO_2 [12] have also been used in FTS for the production of hydrocarbons. Another study [11] on the effects of cerium oxide on the particle size of cobalt, reducibility of cobalt, and catalytic performance of a Co/SiO_2 catalyst shows that the degree of cobalt reduction decreases with the addition of cerium, even in low concentrations.

The kinetic description of the FT reaction is a very important task for industrial practice, being a prerequisite for the industrial process design, optimization, and simulation. The kinetics of cobalt-based FT catalysts has been the subject of many researches for decades. The kinetics of the FTS has been studied extensively to describe the reaction rate using a power law rate equation

* Correspondence: atashi.usb@gmail.com
[1]Department of Chemical Engineering, University of Sistan and Baluchestan, Zahedan 98164-161, Iran
Full list of author information is available at the end of the article

or an equation based on certain mechanistic assumptions. The mechanistic kinetic rate expressions for cobalt catalysts are based on the formation of the monomer species as the rate-determining step in the consumption of synthesis gas. Many kinetic equations have been proposed in the literature for various cobalt catalysts. These equations have been obtained either empirically (using a power law rate equation) or to fit a proposed mechanism [13-18]. Atashi et al. [2], Zennaro et al. [4], Yates and Satterfield [18], and Das et al. [19] have displayed the explicit rate equations based on the Langmuir-Hinshelwood-Hougen-Watson (LHHW) adsorption theory that has been developed for the cobalt-based FT catalysts in tabulated format.

Many studies have been dedicated to the kinetics of FTS catalytic reactions over the mono- and bimetallic catalysts. However, it is particularly important to know that no work on the kinetics of FTS reaction over a Co-Ce catalyst has been performed. Thus, in the present work, for the first time, we attempted to investigate the kinetics and mechanism of the CO hydrogenation on the silica-supported Co-Ce catalyst, which was prepared by co-precipitation procedure. For the kinetic study, a series of statistically representative kinetic data was obtained on a well-characterized silica-supported catalyst over a range of commercial reaction conditions. The kinetics of FT reaction were studied, and the rate expressions were tested against experimental data that was obtained on some selected catalysts. A model was successfully devised, and the kinetic parameters were determined. The catalyst characterization was carried out using different methods including powder X-ray diffraction (XRD), scanning electron microscopy (SEM), and Brunauer-Emmett-Teller (BET) surface area measurements.

Methods

Characterization techniques

Powder XRD measurements were performed using a D8 Advance diffractometer (Bruker AXS, Ettlingen, Germany). Scans were taken with a 2θ step size of 0.02 and a counting time of 1.0 s using a CuK_α radiation source generated at 40 kV and 30 mA. Specimens for XRD were prepared by compaction into a glass-backed aluminum sample holder. Data were collected over a 2θ range from 4° to 70°, and the phases were identified by matching experimental patterns to entries in Diffract^{plus} version 6.0 indexing software. The morphology of the catalysts and their precursors was observed by means of a Cambridge S-360 scanning electron microscope (Cambridge Instruments, Cambridge, England).

BET surface areas, pore volumes, and average pore sizes of the catalyst precursor and calcined samples (before and after the test) were measured by N_2 physisorption using a Quantachrome Nova 2000 automated system (Quantachrome, Boynton Beach, FL, USA). Each catalyst sample was degassed under nitrogen atmosphere at 300°C for 3 h. In order to obtain the BET surface areas, pore volumes, and average pore sizes, different samples were evacuated at −196°C for 66 min.

Fixed-bed reactor system

A schematic representation of the experimental setup is shown in Figure 1. Fischer-Tropsch synthesis was carried out in a fixed-bed micro-reactor made from stainless steel with an inner diameter of 12 mm. Three mass flow controllers (Model 5850E, Brooks Instrument, Hatfield, PA, USA) were used to automatically adjust the flow rate of the inlet gases comprising CO, H_2, and N_2 (purity of 99.99%). The mixture of CO, H_2, and N_2 was subsequently introduced into the reactor, which was placed inside a tubular furnace (Model ATU 150–15, Atbin, Mina Rashid Ave, Dubai). The temperature of the reaction was controlled by a thermocouple inserted into the catalytic bed and visually monitored by a computer. The catalyst was pre-reduced *in situ* at atmospheric pressure under H_2/N_2 flow (N_2/H_2 = 1, flow rate of each gas = 30 $mlmin^{-1}$) at 400°C for 16 h. In each test, 1.0 g of catalyst was loaded, and the reactor operated for about 12 h to ensure that a steady-state operation was attained.

Catalytic evaluation

The experiments were conducted with mixtures of H_2, CO, and nitrogen in a temperature range from 200°C to 300°C and H_2/CO feed ratios of 1:1 and 3:2 (mol/mol) at atmospheric pressure. The arrangements of the parameters and the related levels are shown in Table 1. In all experiments, the space velocities were between 2,700 and 5,200 h^{-1}.

To avoid the effect of deactivation, fresh catalysts were loaded in each experiment. To achieve the isothermal conditions in a catalytic bed, the catalyst was diluted with an inert material (quartz), and axial temperature distribution was ensured using Mear's criterion [20], that is with $L/d_p > 50$. Moreover, the gas hourly space velocity (GHSV) increased to the value in which the CO conversion was almost the same for a variety of catalyst weight, which indicates that film diffusion can be neglected above this GHSV (in this paper, 2,700 h^{-1}). Therefore, the catalyst pellet and the bed can be considered as isothermal. The temperature was also kept constant to within ±1°C by the heater, and the conversion of the reaction was kept low (below 20%) in order not to generate too much heat in the above exothermic reactions. Also, plug flow was assumed for the gaseous feed. The CO

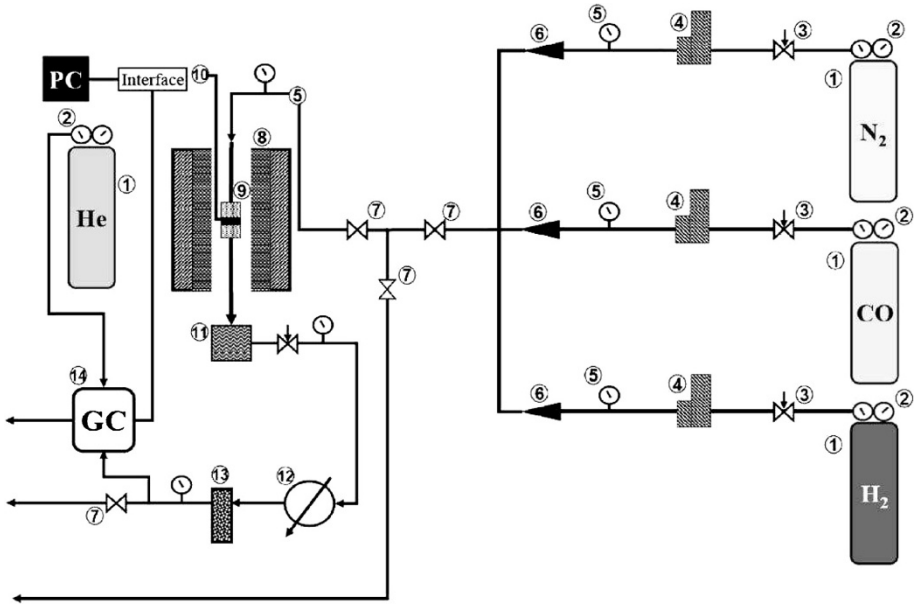

Figure 1 Schematic representation of the reactor used. (1) Gas cylinders, (2) pressure regulators, (3) needle valves, (4) mass flow controllers, (5) monometers, (6) non-return valves, (7) ball valves, (8) tubular furnace, (9) reactor, (10) catalyst bed, (11) trap, (12) condenser, (13) silica gel column, and (14) gas chromatograph (GC).

Table 1 Summary of experimental conditions for the kinetic tests

Number of data	T (°C)	P_{H2} (bar)	P_{CO} (bar)	F/W (mmol g_{cat}^{-1} min^{-1})	X_{CO} (%)	$-rCO$ (mmol g_{cat}^{-1} min^{-1})
1	200	0.333	0.333	0.509	5.83	0.0297
2	210	0.4	0.267	0.498	6.16	0.0306
3	220	0.333	0.333	0.488	8.42	0.0411
4	230	0.4	0.267	0.424	10.21	0.0433
5	240	0.333	0.333	0.469	11.21	0.0526
6	250	0.4	0.267	0.435	12.39	0.0538
7	260	0.333	0.333	0.451	12.40	0.0559
8	270	0.4	0.267	0.443	12.54	0.0555
9	280	0.333	0.333	0.435	12.65	0.055
10	290	0.4	0.267	0.427	12.91	0.0512
11	300	0.333	0.333	0.419	13.19	0.0553
12	200	0.4	0.267	0.407	13.16	0.0535
13	210	0.333	0.333	0.398	13.66	0.0544
14	220	0.4	0.267	0.390	14.46	0.0564
15	230	0.333	0.333	0.450	14.49	0.0652
16	240	0.4	0.267	0.455	16.09	0.0732
17	250	0.333	0.333	0.493	16.28	0.0802
18	260	0.4	0.267	0.282	16.78	0.0474
19	270	0.333	0.333	0.354	17.18	0.0609
20	280	0.4	0.267	0.348	17.94	0.0624
21	290	0.333	0.333	0.342	18.53	0.0633
22	300	0.4	0.267	0.274	19.12	0.0524

P_{tot} = 1 bar after 10 to 15 h of starting the reaction at given conditions.

conversion (%) is calculated according to the normalization method:

$$\text{CO conversion}\ (\%) = \frac{(\text{Moles of CO}_{\text{in}}) - (\text{Moles of CO}_{\text{out}})}{(\text{Moles of CO}_{\text{in}})} \times 100 \quad (1)$$

The experimental reaction rate was determined as follows:

$$\text{Rate of CO conversion} = (\text{Fractional conversion}) \times \frac{(\text{Input flow rate of CO})}{\text{Weight of the catalyst}} \quad (2)$$

Statistical criteria

The unknown parameters for each model were calculated using the experimental data and minimizing the sum of the squares of the differences using the Levenberg-Marquardt algorithm. The experimental reaction rates, the R^2 value (reflects the amount of variance), and the root mean square deviation (RMSD) were used for the evaluation of the fitting.

$$\sigma = \frac{1}{N_{exp}} \sum_{i=1}^{N_{exp}} r_{\text{CO},i}^{exp} \quad (3)$$

$$R^2 = 1 - \left(\frac{\sum_{i=1}^{N_{exp}} \left(r_{\text{CO},i}^{exp} - r_{\text{CO},i}^{cal} \right)^2}{\sum_{i=1}^{N_{exp}} \left(r_{\text{CO},i}^{exp} - \sigma \right)^2} \right)^2 \quad (4)$$

$$\text{RMSD} = \frac{1}{N_{exp}} \left(\sum_{i=1}^{N_{\text{exp}}} \left(r_{\text{CO},i}^{\text{exp}} - r_{\text{CO},i}^{cal} \right)^2 \right)^2 \quad (5)$$

where $r_{\text{CO},i}^{\text{exp}}$ and $r_{\text{CO},i}^{\text{cal}}$ denote the experimental and calculated CO conversion rates using each kinetic model, respectively, and N_{exp} represents the number of experimental data with pure variance σ.

To choose the most suitable kinetic expression, different statistical indices can also be used to determine the quality of regression models. In order to find the most appropriate model, the following conditions should be considered [21]: (1) obtained constants must be positive, (2) coefficients of the equation must obey Arrhenius and van't Houff rules, and (3) the optimal model is the one which gives the highest R^2.

Result and discussion

Catalyst screening results

Characterization of this catalyst was carried out using XRD, and the patterns of this catalyst in different stages of precursor, fresh calcined catalyst (before the test), and used calcined catalyst (after the test) at H_2/CO = 2:1 are shown in Figure 2. The catalyst precursor was found to be amorphous. The presence of amorphous phases in the XRD pattern of the precursor makes the other phases undetectable. However, the calcined catalyst before the test showed different phases, and the actual phases identified in this catalyst were $CoSi_2$ (cubic), CeO_2 (cubic), SiO_2 (monoclinic), $CeCoSiO_2$ (tetragonal), Co_2SiO_4 (cubic), and Co_3O_4 (cubic). In order to identify the changes in the calcined catalyst during the reaction and to detect the phases formed, the catalyst after the test was characterized by XRD and its phases were found to be $CoSi_2$ (cubic), CeO_2 (cubic), CoO (cubic), C (hexagonal), Co_2C (orthorhombic), Ce (hexagonal), Co (hexagonal), and CeC_2 (tetragonal). During chemical reaction, some of the oxidic phases in the calcined catalyst before the test transformed into metallic and carbide phases; and in the tested catalyst, there are oxidic and carbide phases, both of which are active phases in the FTS. Carbide phase is active in CO hydrogenation. Formation of this phase with oxidic phases which are active to olefins cause high performance of supported SiO_2 catalyst [22]. Clearly, the XRD study suggests that the precursor undergoes morphological changing during calcination and also FTS chemical reaction. However, the XRD technique may not be sufficiently sensitive to follow the fine details of these changes. Hence, a detailed SEM study of the precursor and calcined catalysts before and after the test at the optimum molar feed ratio of 2:1 was undertaken, and their SEM images on different stages are presented in Figure 3. The SEM observations showed differences in morphology of the precursor and calcined catalysts (before and after the test). The electron micrograph obtained from the catalyst precursor (Figure 3a) was found to be composed of several agglomerates of particles and shows that this material is less dense. After the calcination at 600°C, the morphological features were different from the precursor sample and showed that the agglomerate measure was greatly reduced compared with the precursor (Figure 3b). It may be due to the calcined catalyst surface that is covered with small crystallites of cobalt and cerium oxide, which is in agreement with the XRD results. After FTS chemical reaction, the catalyst texture and its morphology changed (Figure 3c). However, the size of the grains in the tested catalyst grew larger by agglomeration, which may be due to sintering after reactions. The BET surface area, pore volume, and average pore diameter of the catalysts were tabulated in Table 2. As it can be seen, the calcined catalyst before the test has a higher specific surface area (79 m^2g^{-1}) than its precursor (75 m^2g^{-1}), which is in agreement with the SEM results showing that the agglomerate size of the calcined catalyst is less compared with its precursor and therefore leads to an increase in the BET specific surface area of the calcined sample. The high specific surface area of

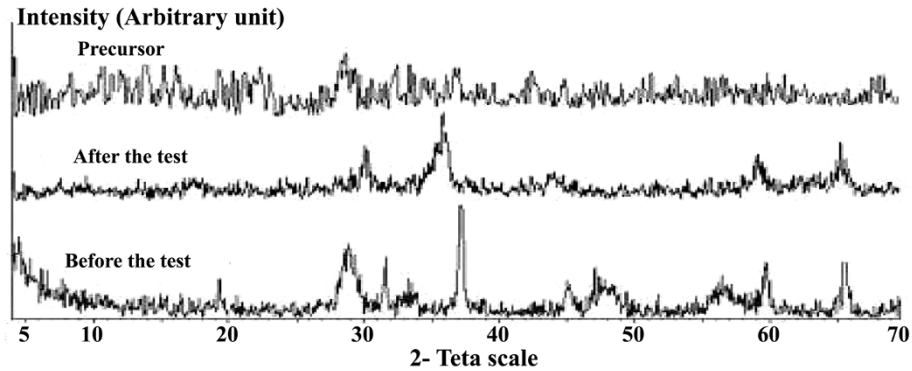

$CoSi_2$	2θ: 29, 48, 57	CeO_2	2θ: 29, 33.5, 48, 57	SiO_2	2θ: 26, 29, 33
CoO	2θ: 37, 42.5	Co_3O_4	2θ: 19, 31, 37, 59, 65.5	Co_2SiO_4	2θ: 19, 37, 45, 49, 59, 65
C	2θ: 41.5, 43, 44	Co_2C	2θ: 37, 39, 59.5, 64.5	Ce	2θ: 32, 36.5, 63
Co	2θ: 41.5, 44.5	CeC_2	2θ: 27, 32.5, 44, 55	$CeCo_2Si_2$	2θ: 37, 46, 59, 60, 66

Figure 2 XRD patterns of precursor and calcined catalysts (before and after the test). Containing 80%Co/20%Ce/15 wt.% SiO_2.

the fresh catalyst before the test allowed a high degree of metal dispersion. The obtained results in Table 2 show that there is no big variation among average pore size diameters of the catalyst in different stages of the precursor and calcined samples (before and after the test).

Development of kinetic equations

CO hydrogenation in FTS process can be analyzed using hydrocarbon chain formation mechanism, which is developed by combining of a number of steps in FTS. The multi-compound product depicts an affluent source of information about the events on the active site by performing high compositional order. Kinetic modeling of the interconnection of surface reaction is an essential step at this point. The mechanism of the hydrocarbon formation during the FTS has been reviewed and discussed by several authors [13,16,23]. On the basis of the nature of CO adsorption and chain initiator intermediates, popular mechanistic proposals include (1) the carbide mechanism [24], wherein CO adsorbs dissociatively and the carbide (Cs) is the chain initiator intermediate, and (2) the enolic mechanism [25], which involves molecular adsorption of CO and the formation of an oxygen intermediate, the enol (HOCs). In the former mechanism, simultaneous dissociative adsorption of CO and H_2 is followed by the hydrogenation of adsorbed carbon by adsorbed hydrogen in a stepwise manner to give methane and higher hydrocarbons. In the latter mechanism, the dissociative adsorption of H_2 and molecular adsorption of CO are followed by the hydrogenation of adsorbed carbon monoxide by adsorbed hydrogen to form an oxygenated intermediate, which reacts with another adsorbed hydrogen to form water and adsorbed carbon, and the reaction of the resulting carbon with adsorbed hydrogen as in the carbide mechanism. For derivation of the LHHW rate expressions, several assumptions were made: (a) The intrinsic reaction rates are proportional to the surface coverage of reactants; (b) CO consumption and $-CH_2$ preparation reaction have one irreversible limiting step, and the other steps were assumed to be quasi-equilibrium; (c) considering steady-state conditions, mediums do not accumulate on the catalyst surface; (d) due to catalyst dilution with quartz, GHSV > 2,700 h^{-1} utilization, and low

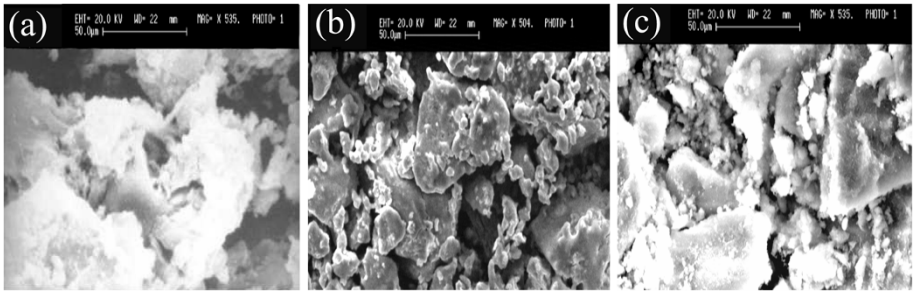

Figure 3 SEM images of the 80%Co/20%Ce/15 wt.% SiO_2catalyst. In the **(a)** precursor,**(b)** catalyst before the test, and **(c)** catalyst after the test at H_2/CO = 2:1.

Table 2 BET results of the precursor and calcined catalysts (before and after the test) containing 80%Co/20%Ce/15wt.%SiO_2

Catalyst	Specific surface area ($m^2\ g^{-1}$)	Pore volume ($cm^3\ g^{-1}$)	Pore size (Å)
Precursor	75.2	2.86×10^{-2}	58.41
Fresh calcined	79.4	6.23×10^{-2}	56.73
Used calcined	53.4	4.63×10^{-2}	60.18

conversion, the operation is assumed to be isothermal; (e) catalysts are fixed and uniformly distributed; (e) the elementary adsorption of hydrogen and carbon monoxide in quasi-equilibrium state within the concentration of gas phase; (f) water is removed irreversibly after CO decomposition; and (g) CO surface concentration is higher compared with hydrogen due to the more difficult adsorption of CO over cobalt catalyst. CO and carbon concentrations are assumed to be dominant concentrations [26-29].

In order to derive rate equations to be adjusted with the data in Table 1, we used the LHHW theory to obtain kinetic models. According to this theory, a reaction mechanism should be adopted. Four mechanisms were offered on the basis of various monomer formations (elementary reactions) and carbon chain distribution pathways. An elementary reaction set on sites for each model is summarized in Table 3.

To derive each kinetic model, one of the elementary reaction (in some case, two or three) steps was assumed as rate-determining step (RDS), and all other steps were considered at equilibrium. Then, all of the models obtained were fitted separately against the experimental data. In the interest of conciseness, only certain selected kinetic models are reported in Table 4.

For example, derivations of the rate equation for FT-IV-2 and FT-I-1 are explained here. The rate expression of the rate-determining step for the FT-IV-2 model, where dissociative H_2 adsorption was the rate-limiting step, can be expressed as irreversible adsorption:

$$-r_{\mathrm{CO}} = k_2 P_{H_2} {\theta_{\mathrm{S}}}^2 \tag{6}$$

where $-r_{\mathrm{CO}}$ is the rate of disappearance of CO, k_2 is the forward rate constant for hydrogen dissociative adsorption, P_{H_2} is hydrogen partial pressure in the gas, and θ_{S} is the empty space fraction. The fraction of vacant sites, θ_{S}, can be calculated from the following balance equation:

$$\theta_{\mathrm{S}} + \theta_{\mathrm{CO}} + \theta_H + \theta_{\mathrm{HCO}} + \theta_C + \theta_{\mathrm{CH}} + \theta_{\mathrm{CH_2}} + \theta_O + \theta_{\mathrm{OH}} = 1. \tag{7}$$

Hydrogen and carbon monoxide adsorbed dissociatively on cobalt catalyst, but depending on the catalyst and reaction condition and the extent of dissociation of CO, their adsorption is varied [30]. However, CO is adsorbed more strongly than hydrogen [31]. In this case, it is assumed that only CO occupies a significant fraction of the total number of sites. Other species were assumed to be negligible in the stoichiometric balance:

$$\theta_{\mathrm{S}} + \theta_{\mathrm{CO}} = 1. \tag{8}$$

The surface coverage of carbon monoxide is calculated from the site balance and the preceding reaction steps which are at quasi-equilibrium:

$$\mathrm{CO} + \mathrm{S} \overset{k_{\mathrm{ads,CO}}}{\leftrightarrow} \mathrm{COs} \tag{9}$$

$$k_{\mathrm{ads,CO}} P_{\mathrm{CO}} \theta_{\mathrm{S}} - k_{\mathrm{des,CO}} \theta_{\mathrm{CO}} = 0 \tag{10}$$

$$\theta_{\mathrm{CO}} = K_1 P_{\mathrm{CO}} \theta_{\mathrm{S}} \tag{11}$$

$$K_1 = \frac{k_{\mathrm{ads,CO}}}{k_{\mathrm{des,CO}}}$$

Table 3 Elementary reaction mechanism set for FTS

Model	Number	Elementary reaction
FT-I	1	$CO + 2s \leftrightarrow Cs + Os$
	2	$H_2 + 2s \leftrightarrow 2Hs$
	3	$Cs + Hs \leftrightarrow HCs + s$
	4	$HCs + Hs \leftrightarrow H_2Cs + s$
	5	$Os + Hs \rightarrow HOs + s$
	6	$HOs + Hs \rightarrow H_2O + 2s$
FT-II	1	$CO + s \leftrightarrow COs$
	2	$H_2 + 2s \leftrightarrow 2Hs$
	3	$COs + s \leftrightarrow Cs + Os$
	4	$Cs + H_2 \leftrightarrow CH_2s$
	5	$Os + H_2 \rightarrow H_2Os$
FT-III	1	$CO + s \leftrightarrow COs$
	2	$COs + H_2 \leftrightarrow H_2COs$
	3	$H_2COs + H_2 \leftrightarrow CH_2s + H_2O$
	4	$H_2 + 2s \leftrightarrow 2Hs$
FT-IV	1	$CO + s \leftrightarrow COs$
	2	$H_2 + 2s \leftrightarrow 2Hs$
	3	$COs + Hs \leftrightarrow HCOs + s$
	4	$HCOs + Hs \leftrightarrow Cs + H_2O + s$
	5	$Cs + Hs \leftrightarrow CHs + s$
	6	$CHs + Hs \leftrightarrow CH_2s + s$
	7	$Os + Hs \rightarrow HOs + s$
	8	$HOs + Hs \rightarrow H_2O + 2s$

Table 4 Reaction rate expressions for the FTS, r_{FT} (mmol g_{cat}^{-1} min^{-1})

Model of rate controlling	Rate equation
FT-I-1	$\frac{k P_{CO}}{\left(1+aP_{CO}^{1/2}+bP_{H_2}^{1/2}\right)^2}$
FT-I-2	$\frac{k P_{H_2}}{\left(1+aP_{CO}^{1/2}+bP_{H_2}^{1/2}\right)^2}$
FT-I-3	$\frac{k P_{CO}^{1/2} P_{H_2}^{1/2}}{\left(1+aP_{CO}^{1/2}+bP_{H_2}^{1/2}\right)^2}$
FT-I-4	$\frac{k P_{CO}^{1/2} P_{H_2}^{3/4}}{\left(1+aP_{CO}^{1/2} P_{H_2}^{-1/4}+bP_{H_2}^{1/2}\right)^2}$
FT-II-1	$\frac{k P_{CO}}{\left(1+aP_{CO}^{1/2}\right)}$
FT-II-2	$\frac{k P_{H_2}}{\left(1+aP_{CO}^{1/2}\right)^2}$
FT-II-3	$\frac{k P_{CO}}{\left(1+aP_{CO}^{1/2}\right)^2}$
FT-II-4	$\frac{k P_{CO}^{1/2} P_{H_2}}{\left(1+aP_{CO}^{1/2}\right)}$
FT-III-1	$\frac{k P_{CO}}{(1+aP_{CO})}$
FT-III-2	$\frac{k P_{CO} P_{H_2}}{1+aP_{CO}}$
FT-III-3	$\frac{k P_{CO} P_{H_2}^2}{1+aP_{CO}}$
FT-IV-1	$\frac{k P_{CO}}{1+aP_{CO}+bP_{H_2}^{1/2}}$
FT-IV-2	$\frac{k P_{H_2}}{(1+aP_{CO})^2}$
FT-IV-3	$\frac{k P_{CO} P_{H_2}^{1/2}}{\left(1+aP_{CO}+bP_{H_2}^{1/2}\right)^2}$
FT-IV-4	$\frac{k P_{CO} P_{H_2}}{\left(1+aP_{CO}+bP_{CO} P_{H_2}^{1/2}\right)^2}$

where K_1 is the equilibrium constant of the CO adsorption step. Substituting Equation 11 into Equation 8, the ratio of free active site can be expressed as:

$$\theta_S = \frac{1}{1 + K_1 P_{CO}} \tag{12}$$

Substituting the fraction of vacant sites into Equation 6, the final rate expression is obtained as follows:

$$-r_{CO} = \frac{k P_{H_2}}{(1 + a P_{CO})^2}. \tag{13}$$

In the same way, the surface fractions (θ) and the final kinetic models would be obtained briefly.

The rate expression of the RDS for model FT-I-1 can be expressed as follows:

$$-r_{CO} = k_1 P_{CO} \theta_S^2 \tag{14}$$

where k_1 is the forward rate constant for carbon monoxide dissociative adsorption, and P_{CO} is carbon monoxide partial pressure in the gas. It is assumed that Cs, Os, and Hs are the abundant surface species, and catalyst site balance is as follows:

$$\theta_S + \theta_C + \theta_O + \theta_H = 1 \tag{15}$$

$$K_1 = \frac{k_1}{k_{-1}} = \frac{\theta_C \theta_O}{P_{CO} \theta_S^2} \tag{16}$$

$$K_2 = \frac{k_2}{k_{-2}} = \frac{\theta_H^2}{P_{H_2} \theta_S^2}. \tag{17}$$

From Equation 16,

$$\theta_O = \frac{K_1 P_{CO} \theta_S^2}{\theta_C}, \tag{18}$$

and from Equation 17,

$$\theta_H = K_2^{0.5} P_{H_2}^{0.5} \theta_S. \tag{19}$$

In steady state, the consumption rate of carbon in stage 3 is equal to the elimination rate of oxygen by stage 5, so

$$k_3 \theta_C \theta_H = k_5 \theta_O \theta_H \Rightarrow \theta_C = \frac{k_5}{k_3} \theta_O. \tag{20}$$

By substituting Equation 18 in Equation 20,

$$\theta_C = \frac{k_5}{k_3} \theta_O = \frac{k_5}{k_3} \left(\frac{K_1 P_{CO} \theta_S^2}{\theta_C} \right) \Rightarrow \theta_C = \left(\frac{k_5 K_1}{k_3} \right)^{0.5} P_{CO}^{0.5} \theta_S, \tag{21}$$

and by substituting Equation 21 in Equation 18,

$$\theta_O = \frac{K_1 P_{CO} \theta_S^2}{\theta_C} = \frac{K_1 P_{CO} \theta_S^2}{\left(\frac{k_5 K_1}{k_3} \right)^{0.5} P_{CO}^{0.5} \theta_S} \Rightarrow \theta_O = \left(\frac{k_3 K_1}{k_5} \right)^{0.5} P_{CO}^{0.5} \theta_S. \tag{22}$$

By substituting Equations 19, 21, and 22 into the site balance equation, the concentration of free active sites will be as follows:

$$\theta_S = \frac{1}{1 + \left(\left(\frac{k_5 K_1}{k_3}\right)^{0.5} + \left(\frac{k_3 K_1}{k_5}\right)^{0.5}\right) P_{CO}^{0.5} + K_2^{0.5} P_{H_2}^{0.5}}, \quad (23)$$

and finally, the rate equation will be as follows:

$$-r_{CO} = \frac{k_1 P_{CO}}{\left(1 + \left(\left(\frac{k_5 K_1}{k_3}\right)^{0.5} + \left(\frac{k_3 K_1}{k_5}\right)^{0.5}\right) P_{CO}^{0.5} + K_2^{0.5} P_{H_2}^{0.5}\right)^2} = \frac{k P_{CO}}{\left(1 + a P_{CO}^{0.5} + b P_{H_2}^{0.5}\right)^2} \quad (24)$$

where $k = k_1$, $a = \left(\left(\frac{k_5 K_1}{k_3}\right)^{0.5} + \left(\frac{k_3 K_1}{k_5}\right)^{0.5}\right)$, and $b = K_2^{0.5}$.

Similar derivations were also made for the other models shown in Table 4. It can be seen that the pressure dependency of CO and H_2on the numerator ranges from 1:2 to 1 and 1:2 to 2, respectively. The denominator is quadratic in case of a dual-site elementary reaction, in contrast to a single-site rate-determining step. The denominator consists of the individual contribution of significantly abundant species on the catalyst surface.

Model parameters and model discrimination

CO consumption rate was obtained from the data in Table 1 by using the differential method of data analysis. The kinetic data presented in Table 1 for CO conversion were used for testing the 15 models listed in Table 4. The least square method and nonlinear regression analysis based on the summarized values in Table 1 were used to determine the kinetic model parameters from the experimental data provided in Table 2. Arrhenius and adsorption equations were substituted in kinetic models: Equations 25 and 26 were substituted for k and a, respectively.

$$k = k_0 \exp\left(\frac{-E}{RT}\right) \quad (25)$$

$$a = a_0 \exp\left(\frac{\Delta H}{RT}\right). \quad (26)$$

According to the statistical results obtained by inserting the data and models, the best model can be selected. Table 5 shows the statistical indicators for the FT kinetic models. Based on the statistical criteria and other conditions [21], and also by comparing the values of R^2, RMSD, and variance, it was recognized that FT-IV-2 is the most appropriate model, which was developed based on enolic mechanism. The model FT-IV shows that the dominant mechanism on the catalyst surface is based on the dissociation of hydrogen with associative adsorbed CO and forming methyl monomers. Although in other studies on cobalt catalyst the dominant mechanism was carbide mechanism, it can be concluded that on

Table 5 Estimated values of the statistical indicators for the FT kinetic models

Model	Kinetic parameter						Statistical indicator		
	k_0 (x) (mmol g^{-1} min^{-1} bar^x)	a_0 (x) (bar^x)	ΔH_a (kJ mol^{-1})	b_0 (x) (bar^x)	ΔH_b (kJ mol^{-1})	E (kJ mol^{-1})	R^2	RMSD (10^{-12})	Variance (10^{-7})
FT-I-1	0.11 (−1)	18.29 (−1/2)	12.25	−91.54 (−1/2)	7.07	−11.27	0.91	5.25	8.328
FT-I-2	2.4E + 03 (−1)	137.35 (−1/2)	7.21	27.05 (−1/2)	7.54	8.49	0.89	5.05	7.578
FT-I-3	0.61 (−1)	−15.41 (−1/2)	4.87	−0.0004 (−1/2)	36.72	2.05	0.78	11.26	38.37
FT-I-4	7.1E + 03 (−5/4)	47.59 (−1/4)	10.02	1.3E + 04 (−1/2)	−18.76	9.86	0.82	10.31	32.13
FT-II-1	9.50 (−1)	1.7E + 04 (−1/2)	40.65			−33.58	0.33	28.06	211.8
FT-II-2	106.97 (−1)	24.43 (−1/2)	1.05			22.22	0.94	5.13	7.071
FT-II-3	765.28 (−1)	1.9E + 03 (−1/2)	5.85			−5.88	0.16	22.34	134.2
FT-II-4	47.34 (−3/2)	86.79 (−1/2)	50.13			−26.36	0.56	16.15	70.11
FT-III-1	12.87 (−1)	6.27 (−1)	33.68			−27.91	0.16	22.34	134.2
FT-III-2	189.18 (−2)	346.87 (−1)	50.04			−26.28	0.56	16.15	70.11
FT-III-3	2.14E + 06 (−3)	1.7E + 03 (−1)	27.64			13.68	0.08	23.35	146.6
FT-IV-1	0.11 (−1)	213.73 (−1)	−13.84	−213.73 (−1/2)	−12.26	25.89	0.93	5.65	9.675
FT-IV-2	8.38 (−1)	15.24 (−1)	−6.55			31.57	0.98	5.05	6.858
FT-IV-3	0.28 (−3/2)	6.42 (−1)	1.24	−18.71 (−1/2)	−5.09	15.94	0.81	5.16	7.726
FT-IV-4	7.68 (−2)	5.85(−1)	10.47	−226.57(−1/2)	−48.91	4.394	0.95	5.28	8.417

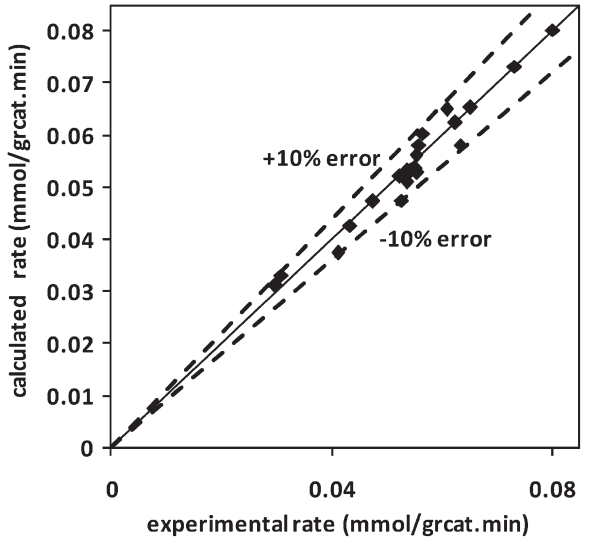

Figure 4 Parity plot of the experimental and calculated CO consumption rates for FT-IV-2.

bimetallic cobalt catalysts, carbon dissociation of CO cannot be done alone. In our previous research on titania-supported Co-Mn catalyst [2], forming the monomer CH_2 was done by reaction of adsorbed CO and hydrogen in two steps, which was assumed as the dominant mechanism. Also, Keyser [32] observed through a study on bimetallic Co-Mn oxide catalyst that a reaction rate equation for the FT reaction based on the enolic mechanism gave results which were marginally better than the results based on the carbide mechanism.

Figure 4 shows a comparison between the experimental data and predicted results of the optimal kinetic model. The solid line in the figure denotes that the calculated $-r_{CO}$ is equal to the experimental one, and the dotted lines over and under the solid line represent 10% deviation. The experimental results were found to be in good agreement with the kinetic model showing about 10% deviation. Therefore, there are appropriate fitting by the LHHW approach in the form of $-r_{CO} = kP_{H_2}/(1 + aP_{CO})^2$. As it has been shown in Table 5 for the best-fitted model (FT-IV-2), the value 31.57 kJmol^{-1} for the activation energy of the Fischer-Tropsch reaction is close to the results reported by Atashi et al. [2].

Experimental

In the present work, we attempted to investigate the kinetics and mechanism of the CO hydrogenation on the silica-supported Co-Ce catalyst, which was prepared by co-precipitation procedure. For the kinetic study, a series of statistically representative kinetic data was obtained on a well-characterized silica-supported catalyst over a range of commercial reaction conditions. The kinetics of Fischer-Tropsch reaction was studied, and the rate expressions were tested against experimental data that were obtained on some selected catalysts.

Materials and processing

The catalyst tested in this study, containing 80%Co/20% Ce/15wt.%SiO_2 which was performed optimally for the conversion of synthesis gas to light olefins [33], was prepared using co-precipitation procedure. Aqueous solutions of $Co(NO_3)_2{\cdot}6H_2O$ (0.5 M) (99%, Merck, White house Station, NJ, USA) and $Ce(NO_3)_3{\cdot}6H_2O$ (0.5 M) (99%, Merck) with different molar ratios were premixed, and the resulting solutions were heated to 70°C in a round-bottomed flask fitted with a condenser. Aqueous Na_2CO_3 (0.5 M) (99.8%, Merck) was added dropwise to the mixed nitrate solution with stirring while the temperature was maintained at 70°C until pH 8 ± 0.1 was achieved. The aged precipitate (120 min) was then filtered and then washed several times with warm distilled water. The precipitate was then dried in an oven at 120°C for 16 h to form a material denoted as the catalyst precursor, which was subsequently calcined in static air in a furnace at 600°C for 6 h to obtain the final catalyst. Then, for the preparation of SiO_2-supported catalyst, the optimal amount of 15 wt.% of SiO_2 based on the total catalyst weight was added to the mixed solution of cobalt and cerium nitrates with the molar ratio of 80%Co/20%Ce and then filtered, washed, dried at 120°C, and calcined at 600°C for 6 h, in the same way as for the unsupported catalyst preparation.

Conclusions

Cobalt-cerium catalyst is an effective catalyst for the hydrogenation of carbon monoxide to light olefins. Experiments for the kinetic of Fischer-Tropsch reaction (hydrocarbon formation) were carried out over the co-precipitated silica-supported Co-Ce catalyst in a fixed-bed micro-reactor over a range of operating conditions. The kinetic models of FTS reaction over a well-characterized 80%Co/20%Ce/15wt.%SiO_2 catalyst, which is used as an optimized catalyst of the process, were studied. The data of this study are best fitted by the simple LHHW approach rate of the form $-r_{CO} = kP_{H_2}/(1 + aP_{CO})^2$ which was developed based on enolic mechanism. The values of the kinetic constants were obtained, and the activation energy was found to be 31.57 kJmol^{-1} for the best model.

Nomenclature

d_p, particle diameter (m); E, activation energy (kJ mol^{-1}); F, molar flow rate (mmol min^{-1}); K, kinetic equation; L, length of the catalytic bed (m); P_i, partial pressure of component i (bar); R, universal gas constant (8.314 J K^{-1} mol^{-1});

RMSD, root mean of standard deviation; R^2, a parameter for goodness of fit; T, temperature (°C); W, catalyst mass (g); ΔH, heat of adsorption (kJ mol^{-1}); $-r_{CO}$, rate constant of the reaction (mmol g_{cat}^{-1} min).

Greek symbols

θ, surface fraction; σ, variance.

Competing interests

The authors declare that they have no competing interests.

Authors' contributions

MM carried out the experiments, studied the mechanism of CO hydrogenation, and analyzed the data with nonlinear regression method. HA and AAM participated in interpretation of results and drafted the manuscript. RJ helped in the experiments and analysis. All the authors have read and approved the final manuscript.

Authors' information

MM is a PhD student of chemical engineering. HA is a professor of chemical engineering. AAM is a professor of chemistry. RJ has an MSc in Chemical Engineering.

Acknowledgements

The authors wish to gratefully acknowledge the helpful comments of Dr. Kiyanoosh Razzaghi and the facilities provided by the University of Sistan and Baluchestan.

Author details

[1]Department of Chemical Engineering, University of Sistan and Baluchestan, Zahedan 98164-161, Iran. [2]Department of Chemistry, University of Sistan and Baluchestan, Zahedan 98135-674, Iran.

Received: 31 August 2012 Accepted: 10 December 2012
Published: 7 January 2013

References

1. Bulavchenko OA, Cherepanova SV, Malakhov VV, Dovlitova LS, Ishchenko AV, Tsybulya SV (2009) *In situ* XRD study of nanocrystalline cobalt oxide reduction. Kinet Catal 50:192–198
2. Atashi H, Siami F, Mirzaei AA, Sarkari M (2010) Kinetic study of Fischer–Tropsch process on titania supported cobalt–manganese catalyst. J Ind Eng Chem 16:952–961
3. Pour AN, Shahri SMK, Bozorgzadeh HR, Zamani Y, Tavasoli A, Marvast MA (2008) Effect of Mg, La and Ca promoters on the structure and catalytic behavior of iron-based catalysts in Fischer–Tropsch synthesis. Appl Catal A Gen 348:201–208
4. Zennaro R, Tagliabue M, Bartholomew C (2000) Kinetics of Fischer–Tropsch synthesis on titania-supported cobalt. Catal Today 58:309–319
5. Mirzaei AA, Shirzadi B, Atashi H, Mansouri M (2012) Modeling and operating conditions optimization of Fischer–Tropsch synthesis in a fixed-bed reactor. J Ind Eng Chem 18:1515–1521
6. Spadaro L, Arena F, Granados ML, Ojeda M, Fierro JLG, Frusteri F (2005) Metal–support interactions and reactivity of Co/CeO_2 catalysts in the Fischer–Tropsch synthesis reaction. J Catal 234:451–462
7. Al-Shammary FY, Caga IT, Tata AY, Winterbotton JM (1991) The effect of CeO_2 support upon activity and selectivity of Ru and Co Fischer Tropsch catalysts. Eur J Solid State Inorg Chem 28:453–456
8. Barault J, Guilleminot A, Achard JC, Paul-Boneour V, Percheron GA, Hilaire L, Coulon M (1986) Syngas reaction over lanthanum-cobalt intermetallic catalysts. Appl Catal A Gen 22:273–287
9. Bruce LA, Hoang M, Hughes AE, Turney TW (1993) Ruthenium promotion of Fischer-Tropsch synthesis over coprecipitated cobalt/ceria catalysts. Appl Catal A Gen 100:51–67
10. Dai X, Yu C, Li R, Shi H, Shen S (2006) Role of CeO_2 promoter in Co/SiO_2 catalyst for Fischer-Tropsch synthesis. Chin J Catal 27:904–910
11. Ernst B, Hilaire L, Kiennemann A (1999) Effects of highly dispersed ceria addition on reducibility, activity and hydrocarbon chain growth of a Co/SiO_2 Fischer–Tropsch catalyst. Catal Today 50:413–427
12. Dai X, Yu C, Shen S (2001) Promotion effect of ceria on Fischer–Tropsch synthesis performance over Co/Al_2O_3. Chin J Catal 22:104–108
13. Jager B, Espinoza R (1995) Advances in low temperature Fischer–Tropsch synthesis. Catal Today 23:17–28
14. Ribeiro FH, Von Wittenau AES, Bartholomew CH, Somorjai GA (1997) Reproducibility of turnover rates in heterogeneous metal catalysis: compilation of data and guidelines for data analysis. Catal Rev Sci Eng 39:49–76
15. Sarup B, Wojciechowski BW (1989) Studies of the Fischer-Tropsch synthesis on a cobalt catalyst. II. kinetics of carbon monoxide conversion to methane and to higher hydrocarbons. Can J Chem Eng 67:62–74
16. Wojciechowski BW (1988) The kinetics of the Fischer-Tropsch synthesis. Catal Rev Sci Eng 30:629–702
17. Yang CH, Massoth FE, Oblad AG (1979) Kinetics of CO + H_2 reaction over co-Cu-Al_2O_3 catalyst. Adv Chem Ser 178:35–46
18. Yates IC, Satterfield CN (1991) Intrinsic kinetics of the Fischer-Tropsch synthesis on a cobalt catalyst. Energy Fuel 5:168–173
19. Das TK, Conner WA, Li J, Jacobs G, Dry ME, Davis BH (2005) Fischer-Tropsch synthesis: kinetics and effect of water for a Co/SiO_2 catalyst. Energy Fuel 19:1430–1454
20. Mollavali M, Yaripour F, Atashi H, Sahebdelfar S (2008) Intrinsic kinetics study of dimethyl ether synthesis from methanol on γ-Al_2O_3 catalysts. Ind Eng Chem Res 47:3265–3277
21. Bercic G, Levec J (1992) Intrinsic and global reaction of methanol dehydration over γ-Al_2O_3 pellets. Ind Eng Chem Res 31:1035–1040
22. Zhang HB, Schrader GL (1985) Characterization of a fused iron catalyst for Fischer-Tropsch synthesis by *in situ* laser Raman spectroscopy. J Catal 5:325–332
23. Iglesia E (1997) Design, synthesis, and use of cobalt-based Fischer–Tropsch synthesis catalysts. Appl Catal A Gen 161:59–78
24. Maitlis PM (1989) A new view of the Fischer–Tropsch polymerization reaction. Pure Appl Chem 61:1747–1754
25. Storch HH, Golumbic N, Aderson RB (1951) The Fischer–Tropsch and related synthesis. Wily, New York
26. Botes FG, Breman BB (2006) Development and testing of a new macro kinetic expression for the iron-based. Ind Eng Chem Res 45:7415–7426
27. Van Der Laan GP, Beenackers AACM (2000) Intrinsic kinetics of the gas-solid Fitscher-Tropsch and water gas shift reactions over a precipitated iron catalyst. Appl Catal A Gen 193:39–53
28. Yang J, Liu Y, Chang J, Wang YN, Bai L, Xu YY, Xiang HW, Li YW, Zhong B (2003) Detailed kinetics of Fischer-Tropsch synthesis on an industrial Fe-Mn catalyst. Ind Eng Chem Res 42:5066–5090
29. Zhang R, Chang J, Xu Y, Cao L, Li Y, Zhou J (2009) Kinetic model of product distribution over Fe catalyst for Fischer-Tropsch synthesis. Energy Fuel 23:4740–4747
30. Ponec V, Van Barnevald WA (1979) The role of chemisorption of Fischer-Tropsch synthesis. Ind Eng Chem Prod Res Dev 18:268–271
31. Christman K, Scober O, Ertl G, Neumann M (1974) Adsorption of CO on a Ni (111) surface. J Chem Phys 60:4719–4724
32. Keyser MJ, Everson RC, Espinoza RL (2000) Fischer–Tropsch kinetic studies with cobalt–manganese oxide catalysts. Ind Eng Chem Res 39:48–54
33. Mirzaei AA, Galavy M, Beigbabaei A, Eslamimanesh V (2007) Preparation and operating conditions for cobalt cerium oxide catalysts used in the conversion of synthesis gas into light olefins. J Iran Chem Soc 4:347–463

doi:10.1186/2228-5547-4-1
Cite this article as: Mansouri *et al.*: **Kinetics of the Fischer-Tropsch synthesis on silica-supported cobalt-cerium catalyst.** *International Journal of Industrial Chemistry* 2013 **4**:1.